Research Article | Vol. 27, No. 22 / 28 October 2019 / Optics Express 31144
Optics EXPRESS

Efficient and environmental-friendly perovskite solar cells via embedding plasmonic nanoparticles: an optical simulation study on realistic device architectures

GEORGE PERRAKIS,[1,2,6] GEORGE KAKAVELAKIS,[3,4,7] GEORGE KENANAKIS,[1] CONSTANTINOS PETRIDIS,[5] EMMANUEL STRATAKIS,[1] MARIA KAFESAKI,[1,2] AND EMMANUEL KYMAKIS[3]

[1] *Institute of Electronic Structure and Laser (IESL), Foundation for Research and Technology Hellas (FORTH), Heraklion, Greece*
[2] *Dept. of Materials Science and Technology, Univ. of Crete, Heraklion, Greece*
[3] *Department of Electrical & Computer Engineering, Hellenic Mediterranean University, Estavromenos, Heraklion, GR-71410 Crete, Greece*
[4] *Cambridge Graphene Centre, University of Cambridge, 9 JJ Thomson Avenue, Cambridge CB3 0FA, UK*
[5] *Department of Electronic Engineering, Hellenic Mediterranean University, Chania GR-71305, Crete, Greece*
[6] *gperrakis@iesl.forth.gr*
[7] *gk415@cam.ac.uk*

Abstract: Solution-processed, lead halide-based perovskite solar cells have recently overcome important challenges, offering low-cost and high solar power conversion efficiencies. However, they still undergo unoptimized light collection due mainly to the thin (~350 nm) polycrystalline absorber layers. Moreover, their high toxicity (due to the presence of lead in perovskite crystalline structures) makes it necessary that the thickness of the absorber layers to be further reduced. Here we address these issues via embedding spherical plasmonic nanoparticles of various sizes, composition, concentrations, and vertical positions, in realistic halide-based perovskite solar cells. We theoretically show that plasmon-enhanced near-field effects and scattering leads to a device photocurrent enhancement up to ~7.3% when silver spheres are embedded inside the perovskite layer. An even further enhancement, up to ~12%, is achieved with the combination of silver spheres in perovskite and aluminum spheres inside the hole transporting layer (PEDOT:PSS). The proper involvement of nanoparticles allows the employment of much thinner perovskite layers (up to 150 nm), reducing thus significantly the toxicity. Providing the requirements related to the design parameters of nanoparticles, our study establishes guidelines for a future development of highly-efficient, environmentally friendly and low-cost plasmonic perovskite solar cells.

1. Introduction

Emerging halide Perovskite ($CH_3NH_3PbX_3$, X = Cl, Br and I) based thin-film Solar Cells (PSCs) have attracted significant interest over the recent years due to their remarkable photovoltaic performance (incident solar to electrical power conversion efficiency of 23.7%). Some of their main characteristics are the high absorption coefficient of perovskite along with its direct band-gap property [1] and, high power conversion efficiency [2,3] (PCE) combined with fabrication simplicity using solution-processing techniques at room temperature [4,5]. However, despite their high performance, there are still two major issues that must be addressed. Firstly, a further improvement of the light collection of the PSCs should be achieved [6,7]. Additionally, a reduction of the PSCs' toxicity [8], due to the presence of pure lead (Pb) in the perovskite materials, should be attained for their further commercialization. A possible solution to reduce

#367241 https://doi.org/10.1364/OE.27.031144
Journal © 2019 Received 13 May 2019; revised 5 Jul 2019; accepted 11 Jul 2019; published 14 Oct 2019

Optics EXPRESS

the amount of the lead is to employ perovskite absorbers thinner than the optimum thickness [9] of about ~350 nm. However, there is a main drawback using this approach, which is the small interaction time of the incoming wave with the very thin perovskite layer, resulting to an unoptimized light collection and thus a reduced absorption.

One of the most promising approaches to increase the light/matter interaction time and as a result to improve light collection in thin-film solar cells is the use of the plasmonic effect [10]. Surface plasmons are collective oscillations of conduction electrons of metallic nanoparticles that are excited by light at the nanoparticle interface with the surrounding dielectric medium. Important features of the surface plasmons are that they are associated with high local-field amplitudes and strong far-field scattering at the resonances of the oscillations. Strong far-field scattering can increase the absorption efficiency in thin film solar cells also by exploiting the effect of total internal reflection. This has been already demonstrated in amorphous-silicon-based thin-film solar cells [11] and in organic solar cells [12]. Moreover, the high local fields in the vicinity of plasmonic nanoparticles overlap not only with metal but also with the surrounding absorbing matter resulting in increased absorption, A. This follows directly from Poynting's theorem for power dissipation [13] [$A \sim |\boldsymbol{E}|^2$]. To benefit from the above features, the parameters determining the resonance characteristics of the plasmonic nanoparticles, i.e. the size, position or the material of the nanoparticles and their hosting environment [14], must be carefully chosen to properly match the plasmon resonance to the spectral properties of the solar cell's material. Otherwise, ohmic losses or coupling between the nanoparticles [15] can lead to increased parasitic absorption in metal turning into heat, a behavior not desirable in solar cells.

Other routes to enhance perovskite solar cell efficiencies have recently proposed in the literature. One prominent example is light focusing structures, such as microlens arrays attached to the top (glass) side of the solar cell [16]. Their main characteristic was the nanoscale light focusing from the microlens within the absorber layer by the formation of vertical standing waves that resulted to enhanced absorption. Another prominent example is inverted vertical-cone photonic-crystal PSC architectures that trap incident sunlight due to parallel-to-interface refraction into slow-light modes over a broad angular range from 0 to 70 degree for both TE and TM linear polarizations [17]. These cases provided significant absorption enhancement even up to 6% compared to the Lambertian limit; however, they require elaborate designs and future commercialization depends on the simplicity of the cell processing.

Already, several studies have explored the plasmonic enhancement in perovskite thin-films [18,19]. An additional reason for this is that metal particles dispersed inside a solution preserve the simplicity of the PSC at processing without increasing its cost [20]. In fact, the cost reduction caused by thickness reduction is greater than that caused by incorporating metal particles. The main finding of the existing studies was that metal particles could improve considerably the beneficial absorption inside the perovskite material [21]. Interestingly, parasitic absorption in metal particles does not surpass the enhancement they provide. More specifically, both N.K. Pathak et al. [22] and Roopak et al. [23] explored Mie theory [24] and showed that silver, gold and aluminum nanoparticles, embedded inside a perovskite matrix, support plasmonic resonances of high magnitude with tunable resonance frequency and width by varying the size, shape or material of the nanoparticles. These results are very promising since plasmonic nanoparticles can induce light incoupling to the perovskite near its band edge (~650-800 nm) where it shows inferior photo response due to lower absorption in conjunction with increased reflection from the perovskite at that regime [6,7]. In this respect, broadband absorption enhancement (>600 nm) was reported in PSCs that incorporated plasmonic gold-silver alloy popcorn-shaped nanoparticles especially around the band-edge, between 720-820 nm. Since the excitation of plasmonic resonances is closely related to the shapes and composition of the metal materials, irregular alloy nanoparticles with many fine structures are conducive to support panchromatic plasmonic resonances [18]. Moreover, Carretero-Palacios S. et al. [25,26] theoretically examined the effect of plasmonic

Optics EXPRESS

enhancement by incorporating metallic nanoparticles of different shapes, sizes, concentrations and composition in methyl ammonium lead iodide perovskite ($CH_3NH_3PbI_3$) absorbing layers assumed to be supported on a glass substrate and coated by a hole transporting material. Notably, it was shown that the conditions for plasmonic enhancement are not very stringent, and ample ranges of sizes, shapes and concentrations of the metallic nanoparticles give rise to an important degree of improvement. In addition, the main conclusion was that the improvement was neatly the result of the near optical field enhancement at longer wavelengths within the absorption band of perovskites (~550-800 nm).

The above-mentioned studies demonstrate the possibility of improvement of perovskite film absorption with the employment of metallic nanoparticles; it is still of great importance, though, if they can be successfully implemented to realistic PSCs. In a real solar cell one has to consider the interplay of metal particles with several optical mechanisms; for instance the effect of the asymmetric environment of the PSC on the localized surface plasmon resonances of the nanoparticles compared to a homogeneous perovskite matrix, coupling with fabry-perrot (FP) resonances (i.e. modes that are supported by the absorbing layer due to its finite thickness) and guided modes of the absorbing layer, interference effects and reflections introduced by the multilayered structure of the PSC, etc., which give rise to a more complex optical system in the neighborhood of the nanoparticles. All those effects are highly unexplored and need careful examination as to definitively conclude on the impact of plasmonic nanoparticles on the performance of realistic PSCs and to be able to optimize this impact.

In this respect we aim in this paper to clarify the effect of the plasmonic nanoparticles on the absorption properties and enhancement of realistic PSCs, with further aim to improve the optical performance of such PSCs. We achieve this by incorporating metal nanoparticles of different size, concentration and material (among the most standard ones, namely silver, gold and aluminum) at different positions into the perovskite absorber or inside different layers of the PSC (see Fig. 1). Moreover, the combined effect of nanoparticles embedded inside different layers at the same time is examined. The aim is to (i) achieve an enhanced absorption efficiency compared to the conventional (nanoparticles-free) PSCs and (ii) reduce the amount of lead by either replacing perovskite material by nanoparticles or by employing thinner perovskite absorbers, without deteriorating the absorption. The perovskite material that we deal with in this work is the most common halide perovskite, the methyl ammonium lead iodide perovskite ($CH_3NH_3PbI_3$), which has been extensively examined for solar cells. One of its main advantages is the fabrication simplicity, while its direct band-gap of ~1.55 eV (~800 nm, i.e. at the onset of the optical range), very close to the ideal compared to other perovskites in which another halide is present, leads to high efficiencies. Improving further its already good performance without increasing the fabrication cost is of high importance.

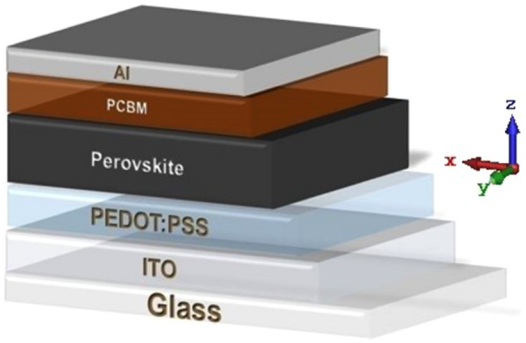

Fig. 1. Geometry of the inverted planar heterojunction perovskite solar cell. The thickness and role of the different layers of the cell are discussed in the main text.

Optics EXPRESS

2. PSC geometrical and material parameters - Modeling approaches

Here we investigate the common inverted [27] planar heterojunction PSC geometry (see Fig. 1) where the poly(3,4-ethylenedioxythiophene) polystyrene sulfonate (PEDOT:PSS) and the phenyl-C71 -butyric acid methyl ester (PCBM) serve as the hole transporting layer (HTL) and the electron transporting layer (ETL) respectively. The planar inverted (upside down fabrication, possibly on top of flexible substrates [27]) PSC adopts the structure of organic solar cells to fulfill the requirements of high performance as well as low-cost and easy fabrication, where all the device layers could be deposited at room temperature through a solution-process [4]. Additionally, since the most efficient two-terminal monolithic Si/Perovskite tandem solar cells are based on inverted heterojunction device architectures, their fine optimization towards the beyond 30% efficiency target is of significant importance. The structure of the device investigated here is as follows: SiO_2 (1.1 mm) /ITO (100 nm) /PEDOT:PSS (40 nm) /$CH_3NH_3PbI_3$ /PCBM (50 nm) /Al (100 nm) (see Fig. 1), where the numbers indicate the thickness of each layer. The transparent conducting oxide (ITO: indium tin oxide) and the aluminum back-reflector serve as the electrical contacts.

In our study the thickness of the perovskite absorber is varied among the standard lengths of PSCs, regarding efficient absorption and photocarrier collection [9], from 150 nm to 400 nm. We note that the optimized perovskite thickness in PSCs is in the range of 280 to 350 nm [28,29]. Larger perovskite thicknesses suffer from long transport distance, which inevitably intensifies adverse recombination, while smaller thicknesses are difficult to demonstrate experimentally due to challenges involved with device fabrication and degradation in electrical properties. However, devices with perovskite thicknesses of ~200 nm have been realized [28] and, as mentioned above, their inadequate light absorption could be sufficiently enhanced.

To simulate the performance of our structures the material parameters used for the perovskite and the materials of the other layers have been obtained from Ref. [4], while those of silver, gold and aluminum from Palik [30]. Despite the "inverted" fabrication sequence of the PSC layers, we will refer as top layers the layers at which the sun is incident on, i.e., following this order from the top to bottom: Glass/ITO/PEDOT:PSS/Perovskite/PCBM/Al.

Due to the complexity of the solar cell geometries investigated here, which include metallic nanoparticles and highly absorbing multilayered materials, a numerical methodology is required. To evaluate the optical performance of the plasmonic PSCs, we performed three-dimensional full-wave electromagnetic simulations using the commercially available software CST Microwave Studio (Computer Simulation Technology GmbH, Darmstadt, Germany) based on the finite element method. Briefly, we assess the optical response of the system by illuminating the structure with a plane wave source at two perpendicular linear polarizations, TE and TM. The simulated structure consists of a semi-infinite SiO_2 (glass) slab, which serves as a substrate for the device fabrication, on top of the multilayered PSC. The simulated region is terminated by unit cell (Floquet) boundary conditions at the bounded planes perpendicular to the surface of the PSC, to investigate the effect of the periodically placed nanoparticles, and by open-boundary (matching) conditions realized by Floquet modes at the unbounded planes parallel to the PSCs' surfaces. Finally, in order to obtain the angular performance, broadband simulations were also performed for each angle of incidence varying from 0 to 70 degrees with a step of 10 degrees.

Finally, we quantify the optical performance of the device with and without the metallic nanoparticles by obtaining numerically the absorption in the perovskite material from which we determine the generated current density inside the solar cell, called the illumination or photocurrent density (J_{ph}), given by:

$$J_{ph} = q \int A_p(\lambda)\Phi_{AM1.5G}(\lambda)d\lambda, \tag{1}$$

In Eq. (1) $\Phi_{\mathrm{AM1.5G}}$ is the photon flux density [in photons·m^{-2}·s^{-1}·nm^{-1}] of the "AM 1.5G" standard sunlight spectrum [31] reaching the Earth's surface, that is considered universal when

Optics EXPRESS

characterizing solar cells, and A_p, q are the absorption of the perovskite material and the elementary charge [in C] of an electron respectively. The integration takes place at $300<\lambda<800$ nm that corresponds to the range within the pass-band edges of the perovskite material. Throughout this work, J_{ph} is considered the most critical parameter for the performance evaluation of the PSCs. Increasing J_{ph} leads to an increased current density under short circuit conditions (J_{SC}) and hence increased extracted electrical power and efficiency, as long as the approach chosen for the J_{ph} enhancement does not have a negative influence on the electrical properties of the device.

In fact, the incorporation of metal nanoparticles in PSCs has been shown that not only is not negative but under certain conditions it can act in favor of the electrical properties of the cell. For instance, as concluded in Ref. [32], the incorporation of metal nanoparticles may preserve or even enhance the diode characteristics of the PSC, like the open-circuit voltage or the fill factor, due to improved transport and collection of charge carriers, as long as a more careful design implementation is applied. Moreover, in plasmonic PSCs larger than the expected photocurrent enhancement was found with the incorporation of core-shell ($Au@SiO_2$) nanoparticles [19]. However, in our study, to ensure that the involvement of nanoparticles will have the smallest possible impact on the electrical properties of the cell, we choose carefully the size and concentration of the nanoparticles when placed close to the carrier transporting layers where an energy barrier for the transportation of the photo-generated carriers can be formed; moreover, the effect of coating layers on the surface of metal nanoparticles, which can cause electrical isolation at metal-semiconductor junctions, is also examined and evaluated.

3. Results and discussion

In the current section we discuss the effect on the PSC photocurrent density (J_{ph}) of plasmonic nanoparticles of spherical shape and of different sizes, concentrations, positions and materials, embedded in different parts of the PSC, for the cell shown in Fig. 1. To gain insight on the mechanisms that lead to the unexploited absorption losses, which decline the absorption efficiency of the solar cell, and to employ a common reference system we investigate and discuss first the pristine PSC, i.e., the cell with no metallic nanoparticles (see subsection 3.1). Next, we discuss the effect of plasmonic spheres inside the perovskite layer of the PSC (subsection 3.2) and demonstrate and analyze the associated increase of photocurrent density. In subsection 3.3 we examine the effect of plasmonic nanoparticles (not only spherical but also cylindrical ones) if placed inside the carrier transporting layers and not in the perovskite layer. This way there is no competition between the volume occupied by the metal particles and the perovskite material. Finally, in subsection 3.4 the combination of nanoparticles placed simultaneously inside more than one layers of the PSC is examined, to demonstrate the full potential of plasmonic nanoparticles if combined with realistic PSCs.

3.1. Pristine PSC

To fully understand the PSC optical response and set appropriate references, we firstly calculate the absorption for each layer of the pristine PSC for a device as shown in Fig. 1 with perovskite layer thickness equal to 350 nm. The result is shown in Fig. 2(a). As can be seen, absorption in perovskite remains high along the entire optical spectrum, due to its high absorption coefficient [see inset in Fig. 2(b)]. Interestingly, high absorption in perovskite persists even at longer wavelengths (~750 nm), close to its band-gap edge (~750-800 nm), as a result of its direct band-gap property. The absorption peak at λ~610 nm is a FP mode arising from the finite thickness of the perovskite slab while the second absorption peak, at λ~750 nm, is a FP mode induced by the aluminum back reflector. Specifically, perovskite absorbs 75% of the maximum achievable current density ($J_{ph,sun}$, obtained from Eq. (1) with A_p=1, integrated at $300<\lambda<800$ nm), while all the other materials of the device absorb 8% (absorption in PCBM is almost zero along the

Optics EXPRESS

entire spectrum). The highest fraction of the unexploited sun spectrum is lost due to reflection and equals 17%.

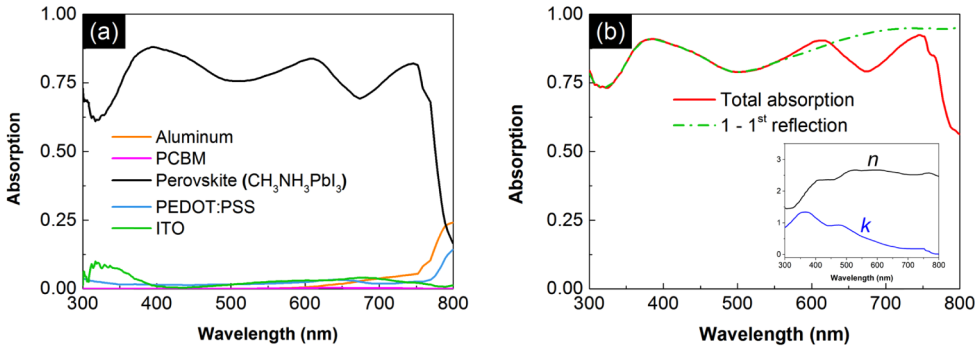

Fig. 2. (a) Absorption in each layer of the PSC. (b) Total absorption (red solid line) of the PSC, absorption in perovskite due to the first reflection only (green dashed-dotted line). Inset: refractive index (black line), n, and absorption coefficient (blue line), k, of perovskite $CH_3NH_3PBI_3$.

To reveal the origin of the reflection losses we calculated both the total absorption (perovskite absorption and the parasitic absorption that occurs at the several layers of the device) of the pristine PSC and the absorption ($A_{1st} = 1 - R_{1st}$) arising from the "first" reflection (R_{1st}) of the top layers of the structure. More specifically, R_{1st} is calculated for the PSC shown in Fig. 1 but assuming a semi-infinite perovskite layer along the z-axis without the back-aluminum reflector and the PCBM layer. This way, the "first" reflection from the top layers can be computationally isolated from the total reflection of the device since waves that are not absorbed and reach the bottom surface of the structure are lost. The result is shown in Fig. 2(b), together with the refractive index and absorption coefficient of the perovskite (see inset – data from Ref. [4]). The red line corresponds to the total absorption (both perovskite absorption and the parasitic absorption that occurs at the several layers of the device) of the pristine PSC (as shown in Fig. 1), which is subject to both multi-pass phenomena and interference effects arising by the multilayer device, and the green line corresponds to the absorption ($A_{1st} = 1 - R_{1st}$) arising from the "first" reflection. As can be seen there, the absorption spectrum of the system is divided into two spectral regimes of different behavior. For λ<550 nm, the total absorption of the pristine PSC follows the absorption arising from the "first" reflection (i.e. it occurs in the first pass of the wave into the perovskite) due to the very high absorption coefficient of the perovskite material for the corresponding wavelengths [see inset in Fig. 2(b)]. For λ>550 nm, where the absorption coefficient of the perovskite material is much lower, interference effects introduced by the several layers of the device of finite thickness are now present, leading to an overall reduced absorption due to higher reflection losses relative to the "first" reflection. These results confirm that further improvement of the PSC could be achieved in agreement with other studies [6,7], at the range of ~650-800 nm where perovskite material shows inferior absorption that results to higher reflection losses from the PSC, as well as at the range of ~350-650 nm by minimizing further the reflection at the PEDOT:PSS-Perovskite interface. Such an improvement can be achieved by adoption of efficient light trapping strategies, which will forbid light from escaping. As we show in this article such a strategy is the proper incorporation of metallic nanoparticles.

Before proceeding to the incorporation of the nanoparticles we evaluate our pristine PSC calculations by comparing with experimental data for the same device [20]. The J_{ph} of our simulated pristine device was calculated at 20.40 mA/cm^2, very close to the experimentally obtained current density under short circuit conditions (J_{SC}), equal to 20.55 mA/cm^2. This

Optics EXPRESS

indicates that the experimental device achieves near-unity quantum yield for the generation and collection of charge carriers [33]. In addition, any mismatch between the simulated sunlight and the AM1.5G standard is negligibly small. The excellent agreement of our theoretical calculations with the experimental measurements allows us to continue with the examination of the plasmonic PSCs while using the J_{ph} of the pristine PSC as a reference.

3.2. Plasmonic nanoparticles inside perovskite

In what follows, we aim to investigate and clarify the effect of plasmonic nanoparticles on the optical response of the PSC for different nanoparticle parameters and configurations. This will allow an efficient understanding and optimization of the PSC performance. In particular, we examine the effect of metal spheres embedded inside the perovskite layer for different metal-material (subsection 3.2.1), sphere size and vertical position (along z-axis, see Fig. 1) (subsection 3.2.2), and sphere lateral-spacing/concentration (subsection 3.2.3), including investigation of features which are likely to be present in a dispersion of metal particles in a realistic PSC, i.e., random particles location and clustering, and other aspects like lattice effects (subsection 3.2.3). Finally, in subsection 3.2.4 the consequences of shielding metal particles with a dielectric coating or covering with organic ligands, an approach commonly employed in realistic systems, are also assessed. In all those studies we assume a constant perovskite layer thickness of 350 nm that is considered optimum regarding the PCE of the PSCs [9]. The spherical shape of nanoparticles was preferred when they are embedded inside the perovskite layer because it is associated with: (i) broadband extinction (scattering and absorption) cross-sections of high magnitude, according to Mie theory [22], for an ample range of diameters, along the entire spectral region near perovskite's band edge (~650-800 nm) where it shows inferior photoresponse; (ii) significant field intensity enhancement in the vicinity of the nanoparticle [23]; (iii) preservation of the PSC fabrication simplicity due to its symmetric nature [34].

3.2.1. PSCs efficiency versus nanoparticle material

Optimization of plasmonic light trapping in solar cells is a balancing act in which several physical parameters and competing factors must be taken into account. For instance, regarding nanoparticle size, very small particles suffer from significant ohmic losses according to Mie theory [24] whereas larger particles, while show larger scattering and smaller ohmic losses, come at the expense of the useful host material (if their spacing is kept constant). Regarding nanoparticle spacing, smaller spacing, associated with larger nanoparticle coupling, may favor absorption (as it may create collective modes propagating in the perovskite), but again comes at the expense of the active perovskite material (if particle size is kept constant). Moreover, one has to take in to account the coupling of nanoparticles with the guided modes supported by the perovskite layer of finite thickness and with the FP resonances induced by the multilayer structure. Thus, the question of optimum size and spacing as to achieve higher nanoparticle-induced PSCs efficiency does not have a trivial answer. Although the above issues will be discussed in more detail in the next sections, while here the aim is to investigate the effect of the nanoparticle metal/composition, it is of great benefit to start our investigation from a nearly optimized size and periodicity setup. For that we performed a "blind" optimization (using the global optimizer of the CST software, employing the "Particle Swarm Optimization" algorithm), requiring maximum photocurrent density enhancement for the plasmonic PSC relative to the pristine PSC (reference system), i.e. maximum $\eta(\%) = ((J_{ph,plasm}\text{-}J_{ph,ref})/J_{ph,ref})\cdot 100$, for spheres of three different metals, namely silver, gold and aluminum. The spheres were forming a square lattice and were located exactly at the middle of the perovskite layer along z-direction (see inset of Fig. 2b). In the optimization the enhancement η was calculated for radius, r, varying from zero to 90 nm and lateral spacing, L (in the x-y-plane), varying from 200 nm to 500 nm. The optimization regarding silver and

Optics EXPRESS

gold spheres gave larger enhancement, η, for $r = 40$ nm, while for aluminum for $r = 60$ nm. The optimum lateral spacing was in all cases $L \sim 300$ nm.

To elucidate the origin of the enhancement and of the above-mentioned optimum parameters, we calculated and plot in Fig. 3(a) the scattering and absorption cross-section for a single silver, gold and aluminum sphere, embedded in perovskite matrix (considering here zero absorption in perovskite). As can be seen in Fig. 3(a), in the region 700-800 nm, where the perovskite shows inferior absorption, the silver and gold spheres (especially silver) present much larger scattering compared to aluminum, indicating their favorable role as plasmonic scatters in plasmonic PSCs. Indeed, this is confirmed by relevant simulations, as those presented in Fig. 3(b).

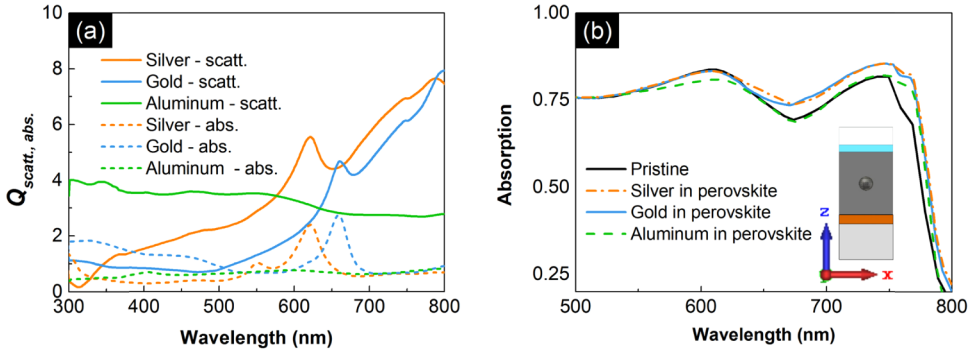

Fig. 3. (a) Scattering (solid lines) and absorption (dashed lines) cross-sections ($Q_{\text{scatt.}, \text{abs}}$) of a silver sphere (orange line – sphere radius 40 nm), gold sphere (blue line- sphere radius 40 nm) and aluminum sphere (green line - sphere radius 60 nm) inside a homogeneous perovskite matrix (here the matrix is considered with no losses and the absorption cross-section represents only ohmic losses inside the spheres); (b) Absorption in perovskite for plasmonic PSCs with silver (orange dashed-dotted line), gold (blue line) and aluminum (green dashed line) spheres placed at the middle of the perovskite layer (see inset) compared to the pristine case (black line). The radii of spheres are as in (a), and they are placed in square lattice with spacing $L = 300$ nm.

Figure 3(b) illustrates the absorption inside the perovskite for plasmonic PSCs that contain silver, gold and aluminum spherical particles located exactly at the middle of the perovskite layer with the size and periodicity for which the photocurrent density was found maximum. As can be concluded from Fig. 3(b), the highest absorption and thus photocurrent enhancement is obtained for silver nanoparticles. Moreover, the absorption enhancement for the case of silver and gold nanoparticles takes place at a wider spectral range compared to aluminum and coincides with the 2nd spectral region (λ>550 nm) mentioned in section 3.1, where the absorption coefficient of the perovskite is lower.

In all cases, the origin of the absorption enhancement was that the plasmonic nanoparticles behaved as light nano-antennas that led to strong scattering (thus to increase of the interaction time of the field with the perovskite material) and to strong local fields (common to plasmonic antennas) in their vicinity, inside the absorptive perovskite layer. These strong local fields are demonstrated in Fig. 4, where the normalized distribution of the squared amplitude of the electric field, $|\boldsymbol{E}|^2/|\boldsymbol{E}_0|^2$, is plotted for an incident plane wave of λ=779 nm, at which the maximum absorption enhancement takes place ($\boldsymbol{E}_0$ is the incident electric field). Figure 4 demonstrates the higher local fields around the sphere for the case of silver and gold nanoparticles compared to the aluminum case. Both high local and scattered fields make the silver nanoparticles the optimum plasmonic material choice for the solar cell absorption enhancement, justifying their corresponding larger enhancement factor [obtained from the data of Fig. 3(b)], which is 3.36%, compared to 2.80% for gold and 0.25% for aluminium.

Optics EXPRESS

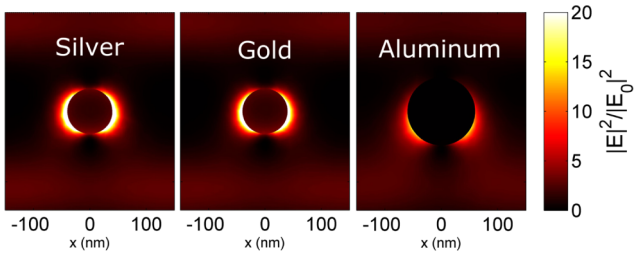

Fig. 4. Normalized (relative to the incident field, E_0) distribution of the squared amplitude of the electric field, at λ=779 nm for silver, gold and aluminum (left, central, right figures respectively) spheres with optimum radius and periodicity for each case.

3.2.2. Vertical position and nanoparticle size effect on the PSCs performance

Another important parameter affecting the optical response of the PSC is the depth at which the nanoparticles are embedded inside the perovskite layer. In a homogeneous perovskite absorbing matrix the effect of nanoparticles' vertical position is related basically to the absorption depth of the wave into the perovskite [25]. For a more complex environment like in PSCs, the effect of nanoparticles' position is not so straightforward and further analysis is needed, given also the fact that in a realistic solar cell device the vertical distribution of nanoparticles is difficult to control. Therefore, in this section, we vary the vertical position (along the z-axis; see Fig. 1) of silver spheres placed in a square lattice in the x-y plane with spacing $L = 300$ nm (spacing for which we have found maximum solar absorption enhancement - see subsection 3.2.1), for two radii; a smaller one, of 40 nm, and a larger, of 70 nm, to take as well into consideration the size effect as the vertical position of nanoparticles varies. Figure 5(a) shows the enhancement factor η (%) as a function of particles' position along the z-direction for $r = 40$ nm (blue line) and $r = 70$ nm (orange line), where Z denotes the distance of the center of the metallic nanoparticle from the top perovskite surface. Figure 5(b) shows the associated absorption spectrum for the case of $r = 40$ nm for vertical distances Z_1=70 nm, Z_2=175 nm (exactly at the middle of the perovskite

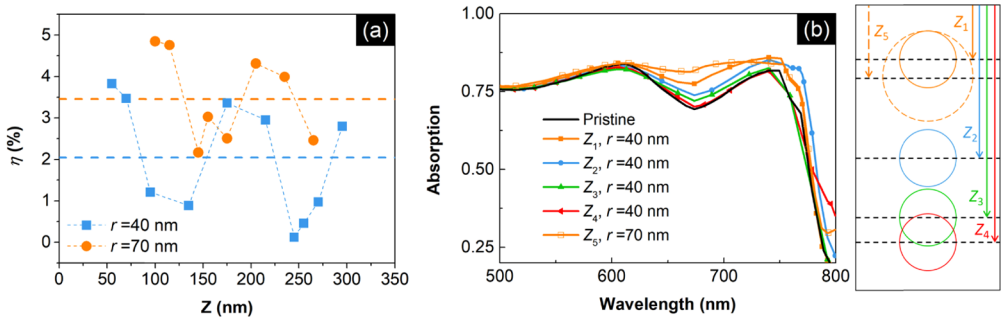

Fig. 5. (a) η (%) as a function of Z which denotes the distance of the center of the metallic nanoparticle from the top perovskite surface, for a periodic (in the x-y plane) system of silver spheres with radius $r = 40$ (blue line) and 70 nm (orange line), and periodicity 300 nm. Dashed lines indicate the averaged η (%) for all positions for each case. (b) Absorption of perovskite for the plasmonic PSC with silver spheres of $r = 40$ nm placed at different vertical positions (Z_1=70 nm – orange line, Z_2=175 nm – blue line, Z_3=245 nm – green line, Z_4=270 nm – red line) inside the perovskite layer, as depicted at the right panel, compared to the case with silver spheres of $r = 70$ nm at Z_5=100 nm (orange dashed line) and the pristine case (black line).

Optics EXPRESS

layer), Z_3=245 nm, Z_4=270 nm (see right panel in Fig. 5), compared to the case with $r = 70$ nm and $Z = Z_5$=100 nm, and with the pristine PSC.

As can be seen, the optimum vertical position is close to the top surface of the perovskite, while the decrease of absorption efficiency going from top to bottoms is not monotonic. In addition, silver spheres of higher radius ($r = 70$ nm) provide higher absorption in most of the vertical positions, and thus higher average η (%) [see dashed lines in Fig. 5(a)].

To reveal the origin of this puzzling non-monotonic behavior as we change the vertical position of the metal nanoparticles inside the perovskite layer, we examined the electric field intensity, $|\boldsymbol{E}|^2/|\boldsymbol{E}_0|^2$, for the $r = 40$ nm case and the vertical positions shown in Fig. 5(b), including the case of the pristine PSC. This intensity for λ=673 nm, where a substantial absorption enhancement is observed, is plotted in Fig. 6.

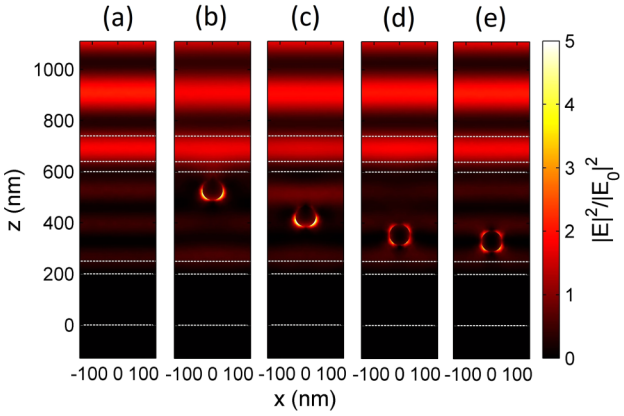

Fig. 6. Normalized distribution of the squared amplitude of the electric field, $|\boldsymbol{E}|^2/|\boldsymbol{E}_0|^2$, at λ=673 nm, for the pristine PSC (a), and for a PSC with spherical silver nanoparticles placed at the four different vertical positions shown in Fig. 5, i.e. at Z_1 (b), Z_2 (c), Z_3 (d), and at Z_4 (e). In all cases the nanoparticles radius is 40 nm and their lateral spacing 300 nm. $\boldsymbol{E}_0$ is the incident electric field.

For the case without nanoparticles, shown in Fig. 6(a), we see that the electric field forms a standing wave inside the perovskite layer which arises from the fabry-perrot resonance induced by the aluminum back reflector of the device. Analyzing the plots shown in Fig. 6, we see that we have larger enhancement in the cases where the vertical nanoparticle position coincides with field maxima of the standing wave, and minimum or no enhancement where the sphere position is in the nodes of the electric field. This is easy to understand taking into account that both the local field around the nanoparticles and the scattered field (main factors of the absorption enhancement) are directly proportional to the input field. Thus, nanoparticles at the field maxima experience the largest possible input field associated with the largest resulting local and scattered fields.

We noticed the same vertical position dependence when spheres of larger size, i.e., with a radius equal to 70 nm, are placed inside the perovskite layer. Moreover, since larger spheres are associated with smaller ohmic losses and larger scattered and near-field enhancement (as they exploit also the quadrupole besides dipole mode), they seem to be more robust regarding their performance associated to their vertical position [see Fig. 5(a)]. Therefore, r~60-70 nm seem to be the optimum sphere size for PSC absorption enhancement.

Interestingly, as observed in Fig. 5(a), the largest absorption enhancement for both the $r = 40$ nm and $r = 70$ nm cases is observed when the spheres are placed close to the top surface of the perovskite. The basic reason is that spheres close to the top of the perovskite behave also as antireflection layer, directing the scattered light towards perovskite. Close to the top of

Optics EXPRESS

the perovskite, the larger scattering offered by the larger size particles seems to lead to larger enhancement [see Fig. 5(b)]. We note though that if placing large metal spheres at the top positions in perovskite, close to the interface with PEDOT:PSS, there is the risk of increasing the interface transport resistance, and therefore a coating layer causing electrical isolation may be needed [35]. The presence and optical response of such a layer is discussed in subsection 3.2.4.

3.2.3. Nanoparticles concentration effect on the PSC performance

In the current section we aim to elucidate the effect of the concentration of metal particles at the expense of the perovskite material. Concentration is considered a critical parameter in plasmonic solar cells since it is a parameter that can be easily controlled externally at processing, while, e.g. the precise control of position is not possible, resulting in a more randomized environment. To predict the effect of the concentration on the solar cell performance and to optimize it, it is not a straightforward task, as this effect is not expected to be monotonic. Small concentrations are expected to give small plasmonic impact while larger concentrations come at the expense of the highly absorbing perovskite material. Here we omit the case of very-closely spaced nanoparticles which requires removal of much of the active perovskite material.

In our numerical study, we change the nanoparticles concentration by changing the lattice constant, i.e., the interparticle distance, maintaining a constant sphere radius ($r = 70$ nm) and vertical position (Z_5 position – see Fig. 5), values/conditions which were found as optimum according to the analysis of our previous sections. The results are shown in Fig. 7, where we plot the absorption versus wavelength for different lattice constants [Fig. 7(a)] and the resulting photocurrent density [Fig. 7(b)].

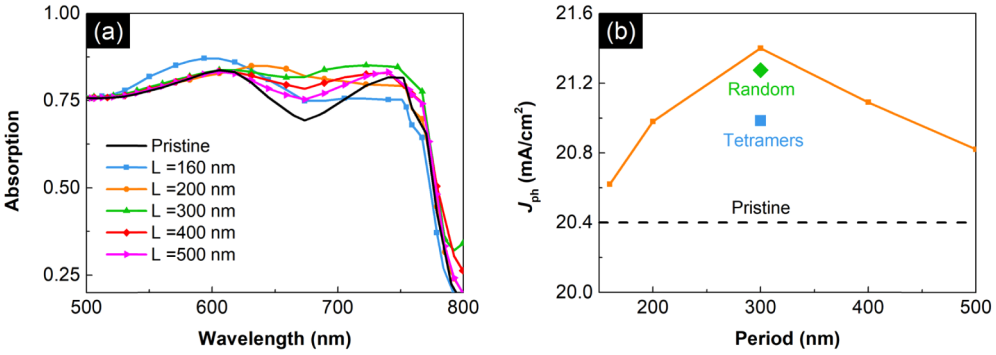

Fig. 7. (a) Absorption of perovskite versus wavelength for different lattice constants (160 nm – blue line; 200 nm – orange line; 300 nm – green line; 400 nm – red line; and 500 nm – magenta line) compared to the pristine case (black line) and (b) the resulting photocurrent density for the different concentrations investigated, assuming silver spheres with a constant radius of 70 nm, and vertical position Z_5 as shown in Fig. 5. The simulations to examine randomness were conducted assuming a periodicity of $L = 2\times300 = 600$ nm (along x-, and y-axis), due to the optimum $L = 300$ nm case of the square lattice, keeping this way the same concentration. Random deviations to the particles lateral position were induced (their spacing in the lateral direction varies randomly thus it is not equal to 300 nm) two times, showing here the results of their average. The result is depicted as the green rhombus. The simulations to examine clustering were conducted assuming again a periodicity of $L = 2\times300 = 600$ nm (along x-, and y-axis), assuming four spheres per unit cell (without altering this way the particles concentration), where we decreased gradually their inter-particle distance going from particles to particle tetramers. The result is depicted as the blue square.

As was expected and mentioned above, the effect of concentration on the photocurrent density is not monotonic. Here lattice constants around 300 nm seem to give the optimum performance,

Optics EXPRESS

while both smaller and larger lattice constants lead to a decline of the achieved photocurrent. This is not unexpected, as mentioned also above, as small concentrations are equivalent to small impact of the plasmonic particles, while larger concentrations are associated also with interparticle coupling and the possible formation of collective modes in the perovskite, which facilitate absorption. Since though the enhancement of concentration goes in conjunction with decrease of the active perovskite material, the effect of the plasmonic enhancement is expected to be overwhelmed above a critical concentration.

The achievement of optimum performance in our case for $L = 300$ nm, where on one hand no very strong interparticle coupling is expected (due to the relatively large interparticle distance) and on the other hand it is still subwavelength compared to the region of 650-750 nm where the plasmonic enhancement has considerable impact, indicates that the effects of deviations from the periodicity of the particles system are expected to be relatively small. This is indeed verified by additional simulations, where we introduced deviations from the periodicity (changing the lateral spheres position) in the system of Fig. 7(a), preserving the concentration of the $L = 300$ nm periodic case; we found a relatively small decrease of the efficiency compared to the periodic case [see green rhombus in Fig. 7(b)]. As was already mentioned examination of non-periodic systems is particularly important in our case, since in realistic solar cells the precise control of the position of nanoparticles is not possible at processing, resulting to a rather random plasmonic system.

Attempting to be as close as possible to the experimentally realizable plasmonic PCSs, in our simulation study we examined also other features which are likely to be present in a dispersion of metal particles in such PSCs, like the effect of clustering. (Although we aim for the precise control of the concentration of nanoparticles inside the perovskite layer, clustering formation during the actual preparation of the films cannot be entirely discarded.) Therefore, we performed simulations assuming a periodicity of $L = 2\times300 = 600$ nm (along x-, and y-axis) with four spheres per unit cell, without altering this way the particles concentration, where we decreased gradually their inter-particle distance going from equally spaced particles to particle tetramers. The impact of clustering for silver spheres of $r = 70$ nm at Z_5 (see Fig. 5) is depicted as the blue square in Fig. 7.

Examining additional concentrations besides the optimum one, we see that although the formation of clustering in general results to a decrease of the solar cell efficiency its effect is not capable to override the plasmonic enhancement. Corresponding field plots showed that the hot spots created inside the inter-particle gap occupy a very small volume that the effect on the perovskite absorption is much less significant than that when particles are separated. However, this balance is better in the case of larger spheres due to the higher scattering, especially when placed close to the top perovskite surface, due to their antireflection property at that position, leading to substantial enhancements even if clustering is present.

3.2.4. Coatings and organic ligands effect on PSCs performance

The preparation of metal (silver, gold, aluminum) nanoparticle dispersions in most fabrication techniques gives nanoparticles covered with ligands (PVP, CTAB, PEG Hexadecylamine) (although there are techniques giving bare nanoparticles, e.g. ultrashort pulsed laser ablation [20]). Moreover, the nanoparticles often are prepared on purpose with dielectric coatings [19,35], e.g. silica, to prevent the direct contact of metal with semiconductor and avoid recombination of the excited charges at the metal/ semiconductor interface. Therefore, it is important to consider also the optical effect of dielectric nanoparticle covering, given the fact that a large part of the plasmon-induced absorption enhancement occurs in the close vicinity of the nanoparticles, i.e. in the area occupied by the coating.

Since, the refractive index of most common organic ligands is almost the same with that of silica, a common dielectric coating, in our optical simulation study the covering of nanoparticles

Optics EXPRESS

will be presumed as silica coating (metal@SiO_2) and can be well accounted for both organic ligands covering and dielectric coating effects.

In Fig. 8 we show the photocurrent enhancement factor η (%) of PSCs containing $r = 40$, 70 nm, $L = 300$ nm silver spheres placed both close to the top perovskite surface (Z_1 for $r = 40$ nm and Z_5 for $r = 70$ nm – see right panel in Fig. 5) and at the middle (Z_2), covered by silica shells of different thicknesses.

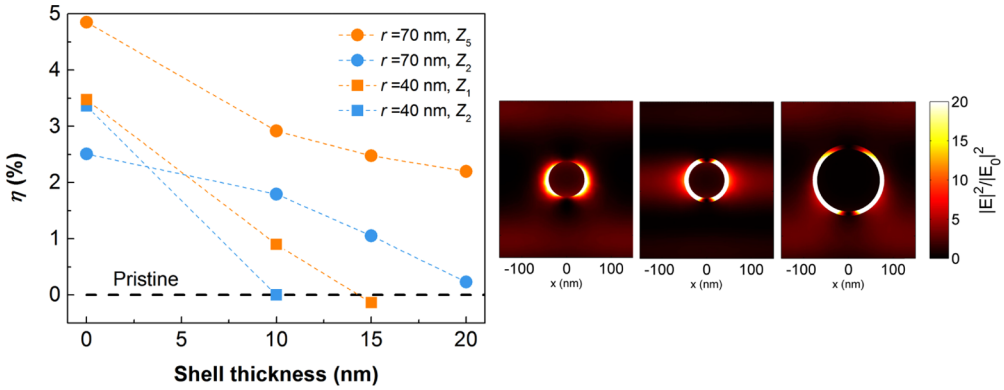

Fig. 8. Photocurrent enhancement factor η (%) of PSCs containing $r = 40$ (lines with squares), 70 nm (lines with circles), $L = 300$ nm silver spheres placed both close to the top surface of the perovskite layer (Z_1 for $r = 40$ nm and Z_5 for r = 70 nm - see right panel in Fig. 5) (orange lines) and at the middle (Z_2) (blue lines) as a function of silica shell thickness, compared to the pristine case. Right panel: Spatial distribution of the normalized electric field intensity at λ=779 nm for silica coated silver spheres (Ag@SiO_2): $r = 40@10$ (middle), $r = 70@10$ (right) compared to the uncoated $r = 40$ nm case (left).

It can be seen that, although the overall light harvesting by the perovskite film is always larger for the uncoated particles case, the presence of a dielectric coating does not necessarily prompt the total collapse of the plasmonic enhancement effect, as long as (i) larger spheres are employed and shell's thickness is not too large, and (ii) especially if the larger spheres are placed close to the top surface of the perovskite layer.

An analysis of the spatial distribution of the calculated electric field intensity ($|\boldsymbol{E}|^2/|\boldsymbol{E}_0|^2$) reveals a strong localization of the optical fields inside the shell, in which no absorption takes place (see right panel in Fig. 8). However, for larger spheres this effect seems to be overwhelmed by their enhanced scattering, leading to maintenance of a high photocurrent enhancement, especially for smaller shell thicknesses (<15 nm). The inferior performance of the coated spheres is related also to another effect of the dielectric coating: it presents a low index environment for the spheres, resulting (especially for thick coatings) to a blue-shift of their plasmonic resonance compared to bare spheres in perovskite. Thus, for spheres showing a plasmonic resonance close to perovskite band edge the coating causes a shift of the resonance towards the high-absorption region of the perovskite where the presence of spheres is not that essential, especially for spheres deeply inside perovskite.

Nevertheless, as mentioned also above, although for most cases shell thicknesses higher than 20 nm should eventually cancel any plasmonic enhancement of the PCS efficiency, this is not the case for the $r = 70$ nm Ag@SiO_2 spheres when placed close to the top of the perovskite surface. This is due to their antireflection property/effect, which is important not only close to the perovskite band-edge but also at lower wavelengths.

Optics EXPRESS

3.3. Plasmonic nanoparticles inside different than the perovskite layers of PSC

Due to the manufacturing procedure of the inverted PSC, the embedding of solution-processed metallic nanoparticles at different layers of the device other than the perovskite, e.g. inside the PEDOT:PSS and the PCBM carrier transporting layers, is possible without increasing the cost [20] as well as maintaining the planar architecture [36]. This way, plasmonic enhancement could be exploited without reducing the perovskite material, albeit at the price of reduced local field enhancement in the absorbing perovskite layer.

Furthermore, placing nanoparticles at the carrier transporting layers may facilitate other internal processes related to the electrical properties of the device. For instance, resonant metallic nanoparticles have been shown to be able to favor the electrical properties of the system too [20,36,37]. Increased exciton generation and dissociation (photocarrier generation, separation) due to the localized surface plasmon resonance oscillating fields that also extend inside the perovskite layer [12], improved carrier transport and extraction due to lower series or contact resistance [20,37] of the solar cell and stability [38] are some examples of the additional impact of plasmonics in PSCs.

In this work we aim first to examine and improve the optical absorption of the PSC by incorporating metal nanoparticles inside the hole-transporting layer, PEDOT:PSS; this way we hope to minimize the reflection at the PEDOT:PSS-Perovskite interface. In the previous discussion we have revealed the importance of the reflection minimization, especially at the PEDOT:PSS-Perovskite interface. Particularly, we showed that the reflection from the multilayered device is the main reason resulting in decreased absorption in perovskite [Fig. 2(b)] along the entire spectrum ($300<\lambda<800$ nm), especially for $\lambda<550$ nm. Interestingly, the low refractive index of PEDOT:PSS ($n\sim1.41$) tunes the plasmonic resonances of metal nanoparticles at lower wavelengths (compared to the case of perovskite host) which coincide with this spectral region. The main restriction in the introduction of nanoparticles in the HTL/ETL is the small thickness of those layers (40, 50 nm) that limits the size of nanoparticles able to maintain the simplicity of the planar architecture. Employing small spheres, though, results to increase of the ohmic losses, as for small spheres absorption dominates extinction. Indeed, embedding spheres of radius $r\sim18$ nm in the PEDOT:PSS enhancement was achieved only for the case of aluminum, with maximum achievable photocurrent $J_{ph}=21.22$ mA/cm^2 [see Fig. 9(a)], corresponding to an enhancement of ~4% (assuming a perovskite layer thickness of 350 nm, and a spheres period of 65 nm). The photocurrent enhancement by embedding the nanoparticles in the PEDOT:PSS layer indicates the possibility to reduce the thickness of the perovskite layer, reducing thus the toxicity of the device (due to the lead content reduction), maintaining though its efficiency. Indeed, as is verified by related simulations, calculating the photocurrent for different perovskite layer thicknesses [see Fig. 9(b)], the thicknesses of about ~270 nm generate the same J_{ph} with that of the conventional (pristine) PSCs with the optimum thickness of ~350 nm. (The step-like behavior of J_{ph} as a function of perovskite thickness at around 275 nm, as observed in Fig. 9(b), is attributed to the appearance of a prominent FP resonance (at $\lambda\sim750$ nm for the 350 nm thickness) as we go from 200 to 300 nm thickness. We have to note that such a step-like response is not present in PSC device architectures with different carrier transport layers [16,39].)

The origin of the absorption enhancement in the case of nanoparticles embedded in the PEDOT:PSS is the re-distribution of the incident light with enhanced scattering in the forward direction (towards the perovskite layer) along with the high local fields which are also extended inside the perovskite layer [see inset in Fig. 9(a)], in conjunction with the low parasitic absorption in aluminum nanoparticles.

Summarizing, we have to note that the antireflection property in PSCs with plasmonic nanoparticles placed in PEDOT:PSS offers a quite prominent absorption enhancement approach, especially at lower wavelengths (<550 nm), because there is no competition between the volume occupied by the metal particles and the absorptive perovskite material. Employing this approach

Optics EXPRESS

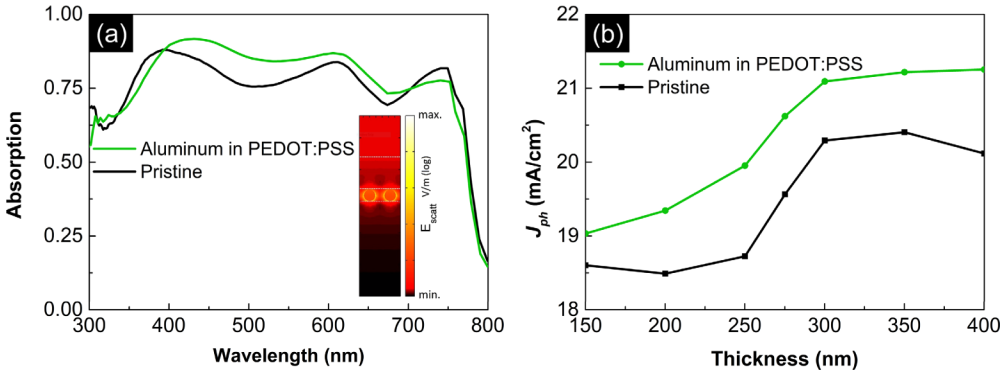

Fig. 9. (a) Absorption in perovskite for the pristine (black line) and the plasmonic PSC (green line) assuming aluminum spheres with radius equal to 18 nm and a period of 65 nm placed inside the PEDOT:PSS carrier transporting layer. The origin of the absorption enhancement is depicted at the right inset where the scattered field, due to the presence of the aluminum nanoparticles, is plotted for λ=517 nm. (b) $J_{\rm ph}$ of the pristine (black line), plasmonic PSC (green line) as a function of the perovskite thickness.

allows employment of thinner perovskite layers, and thus reduction of the structure toxicity, without sacrificing the PSC performance. Placing nanoparticles in PEDOT:PSS is considered a reliable strategy regarding the enhancement of the overall efficiency of the solar cell, since studies have been shown it to favor the electrical properties of the system too [20,36]. In addition, in this case we do not have a decline of the efficiency by coating the particles by a dielectric, i.e. employing Al@SiO_2. This is due to the low refractive index of the PEDOT:PSS matrix, like that of the coating layer.

Regarding incorporation of nanospheres inside the electrons transporting layer (PCBM), we found no enhancement, given the already known nanoparticle size restrictions owing to the small thickness of the ETL, as well as the impossible exploitation of antireflection at lower wavelengths (where the plasmonic resonance of nanospheres in PCBM, with n~2, occurs) in such depth of the PSC, given the highly absorptive nature of perovskite.

An approach to utilize the higher wavelengths (>500 nm) to achieve an efficiency enhancement is to utilize nanoparticles of different shape or different aspect ratio [40] to tailor their localized surface plasmon resonances and tune them at higher wavelengths. The most suitable candidates seem to be the nanorod-shaped particles, because they are synthesized in a wide range of aspect ratios [41] showing two localized dipole resonant modes (aligned with their "short" and "long" axis) and the mode aligned with the axis parallel to the PCBM layer (where no significant size restrictions exist) is highly tunable. The incorporation though of nanorod particles in the ETL layer of our system showed very limited absorption enhancement (due to increased near-field intensity at the vicinity of the nanorods that also extended inside the perovskite material), which was polarization dependent and it is questionable if can be observed in realistic systems (where disorder in the nanoparticle parameters is unavoidable).

Therefore, we conclude that utilizing plasmonic nanoparticles inside the PCBM is not recommended for improving the optical response of the PSCs. Other techniques should be exploited here, i.e., nanostructuring on the back-reflector [42] as long as the interface transport resistance does not increase. Lastly, we note that nanoparticles can be placed inside the ITO layer too with a less harsh size constriction (ITO thickness ~100 nm). However, there they cannot contribute to the increase of the local fields inside the perovskite (since they are far from perovskite), thus their basic role will be to act as antireflectors. For that, nanoparticles of more

Optics EXPRESS

complex geometry [43] or different shape [36] seem to be more appropriate than the spherical ones.

3.4. *Optimizing PSC performance by combining plasmonic particles in different PSC layers*

In this last section of our paper we aim to exploit the full potential of plasmonics in PSCs following our conclusions at earlier parts. This way, an enhanced absorption efficiency, compared to the conventional PSCs (with optimum thicknesses of about ~350 nm) could be achieved as well as the amount of the lead could be further reduced, using thinner perovskite absorbers or replacing perovskite by the nanoparticle material, without deteriorating the absorption.

The first step to explore the possibility of PSCs with reduced lead and high absorption efficiency is to examine and exploit the additive-like absorption behavior of spectrally separated resonances originating from nanoparticles at different PSC layers. For that reason, we utilize the combined effect of both aluminum nanospheres placed inside the PEDOT:PSS layer and of silver spheres located inside the perovskite. Aluminum spheres in PEDOT:PSS provide absorption enhancement at the range of $400<\lambda<700$ nm while silver spheres placed inside the perovskite layer, provide absorption enhancement at the region of $650<\lambda<800$ nm.

Figure 10(a) shows the absorption in perovskite of the combined case compared to the "individual" cases assuming a perovskite layer thickness of ~350 nm. Interestingly, a definite "additive" response is depicted, which is preserved for the whole range of perovskite layer thicknesses, from 400 up to 150 nm [see Fig. 10(b)], confirming the robustness of this approach. Indeed, the enhancement of the combined case equals the sum of the enhancements for only

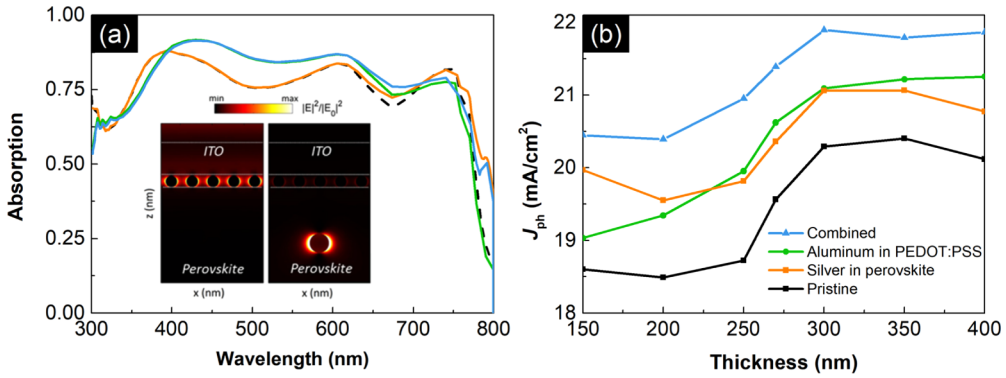

Fig. 10. (a) Absorption in perovskite with thickness equal to 350 nm for the following cases: pristine device (black dashed line), aluminum spheres placed inside the PEDOT:PSS (green line – sphere radius 18 nm, period 65 nm), silver spheres inside the perovskite in the middle (orange line – sphere radius 30 nm, period 325 nm) and their combined case (blue line). Inset: Spatial distribution of the normalized electric field intensity for the combined case at λ=517 nm (left), λ=790 nm (right) verifying the "additive" response of spectrally separated resonances originating from nanoparticles at different PSC layers. (b) J_{ph} as a function of the perovskite thickness for the plasmonic PSCs. The green line corresponds to the case when only aluminum spheres (radius 18 nm, period 65 nm) are placed inside the PEDOT:PSS, the orange line corresponds to the case when only silver spheres are placed in the middle or close to the bottom (position Z_4 of Fig. 5) of the perovskite (with sphere radius of 40 nm and 30 nm respectively, and a period of 300 nm), the blue line shows the effect of the combination of aluminum spheres inside the PEDOT:PSS and silver spheres inside the perovskite in the middle or at Z_4 (with silver sphere radius of 30 nm, and a period of 325 nm); all results are compared to the pristine case (black line).

Optics EXPRESS

silver (in perovskite) and only aluminum (in PEDOT:PSS) spheres. We have to note here that the parameters used in this calculation have been obtained from the optimization studies discussed in the previous sections, but have been modified as to accommodate simulations, to minimize the probability to affect the electrical properties of the PSC and to ensure optimized combined case (i.e. with spheres in both PEDOT:PSS and perovskite layers). Thus, silver spheres of $r = 40$ nm or $r = 30$ nm, placed either in the middle or close to the bottom (position Z_4 of Fig. 5) of the perovskite layer have been employed (minimizing thus the interaction of the spheres in perovskite with those in the PEDOT:PSS), and the silver spheres periodicity in the combined case was considered 325 (i.e. 5×65) nm.

From Fig. 10(b) one can see that for a perovskite layer thickness equal to 150 nm the photocurrent reaches the record value J_{ph}=20.45 mA/cm^2. This result indicates that the lead content reduction can reach values up to 43% (taking into account only the thickness reduction), reducing this way the toxicity of the PSC by a great amount without reducing the photocurrent efficiency compared to conventional pristine PSCs with optimum perovskite thicknesses of about ~350 nm. Regarding the PSC of perovskite thickness 350 nm we found a maximum J_{ph}=21.80 mA/cm^2, corresponding to an enhancement of 6.8% relative to pristine PSC.

We have to note here, that the calculated J_{ph} was even higher than the values shown in Fig. 10(b), and equal to the champion 22.11 mA/cm^2 (~8.4% increase compared to pristine), assuming large silver spheres, with $r = 70$ nm, placed close to the top surface of the perovskite layer (Z_5 see right panel in Fig. 5) with a thickness equal to 350 nm. The results in Fig. 10(b) though correspond to smaller spheres ($r = 30$ nm), owing to the risk of increasing the interface transport resistance employing the larger ones.

Another parameter that is important for solar cell operation is the cell ability to absorb sunlight at off-normal incidence over a wide angular range (without requiring an expensive solar tracking system). To assess the robustness of the optimum parameters concluded in our study for different incidence angles, we calculated the dependence of J_{ph} on the incident angle for some of the above discussed optimum configurations and for the pristine case. The result, averaged over both TE and TM polarizations, is presented in Fig. 11.

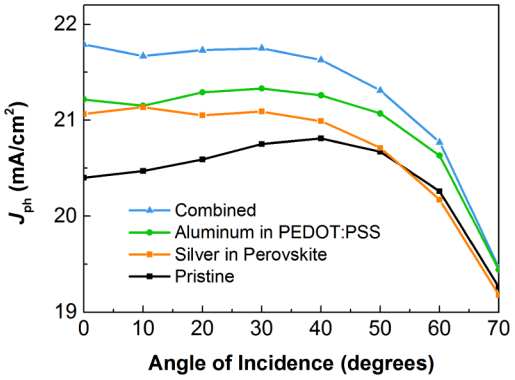

Fig. 11. Dependence of J_{ph} on incident angle averaged over both TE and TM polarizations for the plasmonic PSCs compared to the pristine case. The green line corresponds to the case when only aluminum spheres (radius 18 nm, period 65 nm) are placed inside the PEDOT:PSS, the orange line corresponds to the case when only silver spheres are placed in the middle or close to the bottom (position Z_4 of Fig. 5) of the perovskite (with sphere radius of 40 nm and 30 nm respectively, and a period of 300 nm), the blue line shows the effect of the combination of aluminum spheres inside the PEDOT:PSS and silver spheres inside the perovskite in the middle or close to the bottom (position Z_4 of Fig. 5) (with sphere radius of 30 nm, and a period of 325 nm); all results are compared to the pristine case (black line).

Optics EXPRESS

As can be seen from Fig. 11, the J_{ph} of all plasmonic cases has no substantial degradation for incident angles up to 40 degrees. Moreover, for almost all the angular spectrum all plasmonic cases retain higher J_{ph} compared to the pristine.

4. Conclusions

We examined and discussed here the effect of plasmonic nanoparticles in realistic perovskite solar cells. Placing spherical nanoparticles in different layers of the PSC we examined the possibility to achieve enhancement in the light absorption and thus enhanced photocurrent density, J_{ph}, as well as the related conditions regarding nanoparticle material, size, vertical position and concentration, in particular for nanoparticles embedded in the perovskite layer. Moreover, we examined features that are likely to be present in a dispersion of metal particles in a realistic PSC, i.e. clustering formation and coating layers on the nanoparticles. Our study showed optimum response for silver nanoparticles of radius of around 60-70 nm, especially if placed close to the top of the perovskite layer, while the optimum nanoparticle distance was found to be around 300 nm. The calculated enhancement was found to be quite robust against nanoparticles randomness, polydispersity and angle of incidence. For silver spheres of $r = 70$ nm an average photocurrent enhancement of 3.45%, corresponding to a J_{ph} equal to 21.11 mA/cm^2, was found. The origin of the photocurrent enhancement in all cases was the high local field values associated with the plasmonic resonances (which maximized the absorption), together with the enhanced scattering and antireflection properties of those particles, especially if placed close to the top of the solar cell.

We found considerable photocurrent enhancement (up to 4.0% corresponding to J_{ph}=21.22 mA/cm^2) also for nanoparticles placed in the hole transporting layer (PEDOT:PSS, on top of the perovskite layer) despite the small thickness of that layer and the associated restrictions in the nanoparticle size. The origin of the photocurrent enhancement there was the enhanced scattering in the forward direction (towards the perovskite layer) along with the high local fields which are also extended inside the perovskite layer. Here aluminum nanospheres (of $r = 18$ nm and distance ~65 nm) gave the optimum performance.

The combined effect of placing both aluminum nanospheres in PEDOT:PSS and silver spheres in perovskite resulted at the champion 8.36% absorption enhancement (compared to the pristine case), corresponding to J_{ph} equal to 22.11 mA/cm^2, confirming the additive like absorption behavior of spectrally separated resonances originating from nanoparticles placed at different positions of the solar cell.

The absorption enhancement offered by the plasmonic nanoparticles in PSCs indicates the potential to employ PSCs with quite thin perovskite layers, e.g. 150 nm (thus with reduced toxicity due to the reduced amount of lead), maintaining though the performance of the current PSCs of optimum thickness 350 nm.

Summarizing, we found that embedding metal nanospheres inside realistic PSCs architectures provides a great strategy to improve the optical performance of the device as well as to decrease its toxicity without increasing the cost or the fabrication complexity.

Funding

General Secretariat for Research and Technology (GSRT) (RESEARCH – CREATE – INNOVATE (T1EDK-01082)).

Acknowledgments

This research has been cofinanced by the European Regional Development Fund of the European Union and Greek national funds through the Operational Program Competitiveness, Entrepreneurship and Innovation, under the call RESEARCH – CREATE – INNOVATE (project code:T1EDK-01082).

Optics EXPRESS

References

1. N. K. Kumawat, M. N. Tripathi, U. Waghmare, and D. Kabra, "Structural, optical, and electronic properties of wide bandgap perovskites: experimental and theoretical investigations," J. Phys. Chem. A **120**(22), 3917–3923 (2016).
2. A. Kojima, K. Teshima, Y. Shirai, and T. Miyasaka, "Organometal halide perovskites as visible-light sensitizers for photovoltaic cells," J. Am. Chem. Soc. **131**(17), 6050–6051 (2009).
3. *NREL Best research-cell photovoltaic efficiency chart*., (n.d.).
4. G. Kakavelakis, T. Maksudov, D. Konios, I. Paradisanos, G. Kioseoglou, E. Stratakis, and E. Kymakis, "Efficient and highly air stable planar inverted perovskite solar cells with reduced graphene oxide doped PCBM electron transporting layer," Adv. Energy Mater. **7**(7), 1602120 (2017).
5. G. Kakavelakis, I. Paradisanos, B. Paci, A. Generosi, M. Papachatzakis, T. Maksudov, L. Najafi, A. E. Del Rio Castillo, G. Kioseoglou, E. Stratakis, F. Bonaccorso, and E. Kymakis, "Extending the continuous operating lifetime of perovskite solar cells with a molybdenum disulfide hole extraction interlayer," Adv. Energy Mater. **8**(12), 1702287 (2018).
6. M. Anaya, G. Lozano, M. E. Calvo, W. Zhang, M. B. Johnston, H. J. Snaith, and H. Míguez, "Optical description of mesostructured organic–inorganic halide perovskite solar cells," J. Phys. Chem. Lett. **6**(1), 48–53 (2015).
7. Q. Lin, A. Armin, R. C. R. Nagiri, P. L. Burn, and P. Meredith, "Electro-optics of perovskite solar cells," Nat. Photonics **9**(2), 106–112 (2015).
8. A. H. Slavney, R. W. Smaha, I. C. Smith, A. Jaffe, D. Umeyama, and H. I. Karunadasa, "Chemical approaches to addressing the instability and toxicity of lead–halide perovskite absorbers," Inorg. Chem. **56**(1), 46–55 (2017).
9. L. J. Phillips, A. M. Rashed, R. E. Treharne, J. Kay, P. Yates, I. Z. Mitrovic, A. Weerakkody, S. Hall, and K. Durose, "Maximizing the optical performance of planar $CH_3NH_3PbI_3$ hybrid perovskite heterojunction stacks," Sol. Energy Mater. Sol. Cells **147**, 327–333 (2016).
10. H. A. Atwater and A. Polman, "Plasmonics for improved photovoltaic devices," Nat. Mater. **9**(3), 205–213 (2010).
11. H. Tan, R. Santbergen, A. H. M. Smets, and M. Zeman, "Plasmonic light trapping in thin-film silicon solar cells with improved self-assembled silver nanoparticles," Nano Lett. **12**(8), 4070–4076 (2012).
12. G. Kakavelakis, I. Vangelidis, A. Heuer-Jungemann, A. G. Kanaras, E. Lidorikis, E. Stratakis, and E. Kymakis, "Plasmonic backscattering effect in high-efficient organic photovoltaic devices," Adv. Energy Mater. **6**(2), 1501640 (2016).
13. J. D. Jackson, *Classical Electrodynamics* (Wiley, 1999).
14. C. Noguez, "Surface plasmons on metal nanoparticles: the influence of shape and physical environment," J. Phys. Chem. C **111**(10), 3806–3819 (2007).
15. J. R. Krenn, A. Dereux, J. C. Weeber, E. Bourillot, Y. Lacroute, J. P. Goudonnet, G. Schider, W. Gotschy, A. Leitner, F. R. Aussenegg, and C. Girard, "Squeezing the optical near-field zone by plasmon coupling of metallic nanoparticles," Phys. Rev. Lett. **82**(12), 2590–2593 (1999).
16. A. Peer, R. Biswas, J.-M. Park, R. Shinar, and J. Shinar, "Light management in perovskite solar cells and organic LEDs with microlens arrays," Opt. Express **25**(9), 10704 (2017).
17. Q. G. Du, G. Shen, and S. John, "Light-trapping in perovskite solar cells," AIP Adv. **6**(6), 065002 (2016).
18. Z. Lu, X. Pan, Y. Ma, Y. Li, L. Zheng, D. Zhang, Q. Xu, Z. Chen, S. Wang, B. Qu, F. Liu, Y. Huang, L. Xiao, and Q. Gong, "Plasmonic-enhanced perovskite solar cells using alloy popcorn nanoparticles," RSC Adv. **5**(15), 11175–11179 (2015).
19. W. Zhang, M. Saliba, S. D. Stranks, Y. Sun, X. Shi, U. Wiesner, and H. J. Snaith, "Enhancement of perovskite-based solar cells employing core–shell metal nanoparticles," Nano Lett. **13**(9), 4505–4510 (2013).
20. G. Kakavelakis, K. Alexaki, E. Stratakis, and E. Kymakis, "Efficiency and stability enhancement of inverted perovskite solar cells via the addition of metal nanoparticles in the hole transport layer," RSC Adv. **7**(21), 12998–13002 (2017).
21. B. Cai, Y. Peng, Y.-B. Cheng, and M. Gu, "4-fold photocurrent enhancement in ultrathin nanoplasmonic perovskite solar cells," Opt. Express **23**(24), A1700 (2015).
22. N. K. Pathak and R. P. Sharma, "Study of broadband tunable properties of surface plasmon resonances of noble metal nanoparticles using mie scattering theory: plasmonic perovskite interaction," Plasmonics **11**(3), 713–719 (2016).
23. S. Roopak, A. Ji, P. K. Parashar, and R. P. Sharma, "Light incoupling tolerance of resonant and nonresonant metal nanostructures embedded in perovskite medium: effect of various geometries on broad spectral resonance," J. Phys. D: Appl. Phys. **50**(33), 335105 (2017).
24. J. Stratton, *Electromagnetic theory* (Wiley-IEEE Press, 2007).
25. S. Carretero-Palacios, M. E. Calvo, and H. Míguez, "Absorption enhancement in organic–inorganic halide perovskite films with embedded plasmonic gold nanoparticles," J. Phys. Chem. C **119**(32), 18635–18640 (2015).
26. S. Carretero-Palacios, A. Jiménez-Solano, and H. Míguez, "Plasmonic nanoparticles as light-harvesting enhancers in perovskite solar cells: a user's guide," ACS Energy Lett. **1**(1), 323–331 (2016).
27. P. Docampo, J. M. Ball, M. Darwich, G. E. Eperon, and H. J. Snaith, "Efficient organometal trihalide perovskite planar-heterojunction solar cells on flexible polymer substrates," Nat. Commun. **4**(1), 2761 (2013).
28. Z. Xiao, C. Bi, Y. Shao, Q. Dong, Q. Wang, Y. Yuan, C. Wang, Y. Gao, and J. Huang, "Efficient, high yield perovskite photovoltaic devices grown by interdiffusion of solution-processed precursor stacking layers," Energy Environ. Sci. **7**(8), 2619–2623 (2014).
29. R. Wu, J. Yang, J. Xiong, P. Liu, C. Zhou, H. Huang, Y. Gao, and B. Yang, "Efficient electron-blocking layer-free planar heterojunction perovskite solar cells with a high open-circuit voltage," Org. Electron. **26**, 265–272 (2015).

Optics EXPRESS

30. E. D. Palik, *Handbook of Optical Constants of Solids. II* (Academic Press, 1998).
31. *Solar Spectral Irradiance: Air Mass 1.5*, https://rredc.nrel.gov/solar/spectra/am1.5/.
32. G. Kakavelakis, K. Petridis, and E. Kymakis, "Recent advances in plasmonic metal and rare-earth-element upconversion nanoparticle doped perovskite solar cells," J. Mater. Chem. A **5**(41), 21604–21624 (2017).
33. J. Burschka, N. Pellet, S.-J. Moon, R. Humphry-Baker, P. Gao, M. K. Nazeeruddin, and M. Grätzel, "Sequential deposition as a route to high-performance perovskite-sensitized solar cells," Nature **499**(7458), 316–319 (2013).
34. M. Omelyanovich, S. Makarov, V. Milichko, and C. Simovski, "Enhancement of perovskite solar cells by plasmonic nanoparticles," Mater. Sci. Appl. **7**, 836–847 (2016).
35. R. Wu, B. Yang, C. Zhang, Y. Huang, Y. Cui, P. Liu, C. Zhou, Y. Hao, Y. Gao, and J. Yang, "Prominent efficiency enhancement in perovskite solar cells employing silica-coated gold nanorods," J. Phys. Chem. C **120**(13), 6996–7004 (2016).
36. H.-L. Hsu, T.-Y. Juang, C.-P. Chen, C.-M. Hsieh, C.-C. Yang, C.-L. Huang, and R.-J. Jeng, "Enhanced efficiency of organic and perovskite photovoltaics from shape-dependent broadband plasmonic effects of silver nanoplates," Sol. Energy Mater. Sol. Cells **140**, 224–231 (2015).
37. Z. Sun, Y. Xiahou, T. Cao, K. Zhang, Z. Wang, P. Huang, K. Zhu, L. Yuan, Y. Zhou, B. Song, H. Xia, and N. Chen, "Enhanced p-i-n type perovskite solar cells by doping AuAg@AuAg core-shell alloy nanocrystals into PEDOT:PSS layer," Org. Electron. **52**, 309–316 (2018).
38. N.-G. Park, "Perovskite solar cells: an emerging photovoltaic technology," Mater. Today **18**(2), 65–72 (2015).
39. J. M. Ball, S. D. Stranks, M. T. Hörantner, S. Hüttner, W. Zhang, E. J. W. Crossland, I. Ramirez, M. Riede, M. B. Johnston, R. H. Friend, and H. J. Snaith, "Optical properties and limiting photocurrent of thin-film perovskite solar cells," Energy Environ. Sci. **8**(2), 602–609 (2015).
40. S. Eustis and M. A. El-Sayed, "Determination of the aspect ratio statistical distribution of gold nanorods in solution from a theoretical fit of the observed inhomogeneously broadened longitudinal plasmon resonance absorption spectrum," J. Appl. Phys. **100**(4), 044324 (2006).
41. B. Nikoobakht and M. A. El-Sayed, "Preparation and growth mechanism of gold nanorods (nrs) using seed-mediated growth method," Chem. Mater. **15**(10), 1957–1962 (2003).
42. T. Shen, S. Siontas, and D. Pacifici, "Plasmon-enhanced thin-film perovskite solar cells," J. Phys. Chem. C **122**(41), 23691–23697 (2018).
43. W. Liu, J. Zhang, B. Lei, H. Ma, W. Xie, and H. Hu, "Ultra-directional forward scattering by individual core-shell nanoparticles," Opt. Express **22**(13), 16178 (2014).